Analytica Chimica Acta 1249 (2023) 340948

Contents lists available at ScienceDirect

Analytica Chimica Acta

journal homepage: www.elsevier.com/locate/aca

High temperature total consumption sample introduction system coupled to microwave plasma optical emission spectrometry (MIP-OES) for the analysis of aqueous samples

Santiago Martínez, Raquel Sánchez *, José-Luis Todolí

Department of Analytical Chemistry, Nutrition and Food Sciences, University of Alicante, 03690, San Vicente del Raspeig, Alicante, Spain

HIGHLIGHTS

- Adaptation of a high temperature sample introduction system (hTISIS) to MIP-OES.
- A simple, rapid and accurate method allows trace elements determination.
- Matrix effect mitigation allows accurate analysis by applying external calibration using a set of plain water standards.
- Analysis of samples according to a continuous sample aspiration regime allows its application as a routine method.

GRAPHICAL ABSTRACT

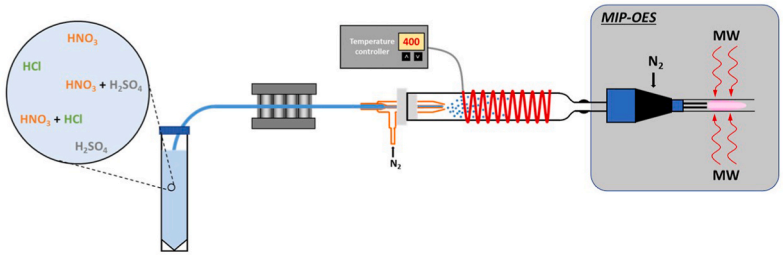

ARTICLE INFO

Keywords:
Digested samples analysis
Oil and fats analysis
MIP-OES
High temperature sample introduction system (hTISIS)
Matrix effects

ABSTRACT

The high temperature torch integrated sample introduction system (hTISIS) is coupled to microwave plasma optical emission spectrometry (MIP-OES) for the first time. The goal of this work is to develop an accurate analysis of digested samples under continuous sample aspiration mode by coupling the hTISIS to a MIP-OES instrument. To achieve this, different operating conditions such as, nebulization flow rate, liquid flow rate and the spray chamber temperature were optimized in terms of sensitivity, limits of quantification (LOQs) and background equivalent concentration (BECs) for the determination of Ca, Cr, Cu Fe, K, Mg, Mn, Na, Pb and Zn, and these values were compared with those reported with a conventional sample introduction system. Under optimum conditions (0.8–1 L min^{-1}, 100 μL min^{-1} and 400 °C, respectively), the hTISIS improved MIP-OES analytical figures of merit and shortened 4-times wash out times with respect to a conventional cyclonic spray chamber, reporting an enhancement factor in the sensitivity among 2–47 times and LOQs from 0.9 to 360 μg kg^{-1}. Once the best operating conditions were set, the magnitude of the interference caused by 15 different acid matrices (2, 5 and 10% w/w of HNO_3, H_2SO_4, HCl and mixtures of HNO_3 with H_2SO_4 and HNO_3 with HCl) was significantly lower for the former device. Finally, 6 different digested oily samples (used cooking oil, animal fat, corn oil and the same samples after a filtration step) were analyzed by means of an external calibration approach based on the use of multielemental standards prepared in 3% (w/w) HCl solution. The obtained results were compared against those supplied by a conventional methodology employing an inductively coupled plasma optical emission spectrometry, ICP-OES, instrument. It was clearly concluded that the hTISIS coupled to MIP-OES afforded similar concentrations as compared to the conventional methodology.

* Corresponding author.
E-mail address: r.sanchez@ua.es (R. Sánchez).

https://doi.org/10.1016/j.aca.2023.340948
Received 26 September 2022; Received in revised form 10 January 2023; Accepted 5 February 2023
Available online 6 February 2023

1. Introduction

Spectroscopic techniques are commonly employed to carry out the elemental analysis of inorganic as well as organic samples. Among them, flame atomic absorption spectrometry (FAAS), electrothermal atomic absorption spectrometry (ETAAS), inductively coupled plasma optical emission spectroscopy (ICP-OES) and inductively coupled plasma mass spectrometry (ICP-MS) are normally the most used techniques [1]. Within this context, microwave induced plasma optical emission spectrometry (MIP-OES), is being increasingly applied to carry out multielemental analysis of samples of interest for areas such as: energy [2], agriculture [3], pharmacology [4], geology [5] and food [6], since this technique reports: *(i)* lower limits of detection (LODs) and wider dynamic ranges than FAAS, and similar values of these parameters to those afforded by ICP-OES; *(ii)* higher sample throughput than FAAS due to its multielemental capability; *(iii)* smaller footprint, less expensive and low maintenance costs than an ICP-OES instrument because nitrogen can be used instead of argon as plasma gas. Moreover, the nitrogen gas supply can originate from a generator instead of from cylinders or liquid storing systems, thus increasing the instrument autonomy [7–9], and, *(iv)* Nitrogen microwave plasmas are more robust to organic samples such as crude and lubricating oils than argon plasmas [10,11]. Furthermore, this kind of plasma reaches the local thermodynamic equilibrium (LTE) faster than an argon plasma [12,13].

There are two ways of generating a plasma using microwave radiation. On the one hand, the capacitively-coupled microwave plasma (CMP), in which the plasma is generated at the tip of an electrode by applying microwave radiation. On the other hand, the microwave-induced plasma (MIP), in which the plasma is inductively created inside of a resonant cavity containing a neutral gas, without any dielectric contact [14]. However, the former instruments showed poor sensitivities, low plasma temperatures and troubles handling liquid aerosols due to the low microwave power applied (<300 W) and the non-toroidal plasma shape [15].

With the development of new microwave plasma geometries, such as the Microwave Plasma Torch (MPT), Okamoto and Hammer cavities, high-power instruments were set, and nebulized solutions could be introduced into the plasma. In 2011, a commercial instrument was introduced by Agilent Technologies (4100 MP-AES), which combined a Hammer cavity with a resonant iris cavity and Nitrogen as plasma gas [12,16]. The use of a Czerny-Turner monochromator with a CCD detector allowed this instrument to be applied for sequential instead of simultaneous analysis. However, as an advantage, this configuration permits the selection of an optimal nebulization gas flow rate and a plasma viewing position for each analyte [17].

Because the power to generate the plasma is limited at 1000 W in the commercial MIP-OES, the plasma temperature in these instruments is lower (4200–5400 K) than those obtained for ICP instruments (around 7500 K). Therefore, the thermal decomposition of the sample may be incomplete, and some elements are not efficiently ionized, being preferable the selection of atomic emission lines for the analyte determination [18]. Moreover, Mg II/Mg I values (between 0.26 and 2.01) are lower than ICP plasmas and, hence, different calibration methodologies, such as matrix-matching, internal standard and standard addition, are employed to ensure accurate analysis of complex matrix samples [13,19]. In fact, strong matrix effects are reported in MIP-OES, especially when the samples contain high concentrations of easily ionized elements (EIEs) [16,19,20].

In order to improve the analytical figures of merit and to lower the intensity of matrix effects related to the analyte transport efficiency to the plasma, the sample introduction system can be modified. In this context, the so-called high temperature torch integrated sample introduction system (hTISIS) might be a good alternative to carry out this kind of analysis. The system consists of a low inner volume single-pass spray chamber whose walls are heated by means of an electric resistance. Under optimized conditions, the analyte transport efficiency becomes virtually equal to 100% regardless of the sample matrix, thus improving the sensitivity provided by conventional devices and, simultaneously, reducing the extent of the matrix effects related to the spray chamber [21].

Up to now, the hTISIS has been employed to analyze aqueous [22] and organic samples [23] by ICP-OES and ICP-MS. Nevertheless, this device has never been coupled to an MIP-OES instrument. The goal of the present work was thus to evaluate the analytical performance of the hTISIS as a liquid sample introduction system for MIP-OES. Analytical figures of merit (*i.e.*, sensitivity, LOQs and BECs) have been compared with those for a conventional sample introduction system. Furthermore, the extent of matrix effects caused by inorganic acids has also been characterized. Finally, as an example of an analytical application, the hTISIS has been used to the analysis of digested real oil and grease samples.

2. Experimental

2.1. Reagents and samples

All solutions were diluted in high-purity water, ≥18.2 MΩ cm, obtained from a Milli-Q water IQ 7000 purification system (Millipore Inc., Paris, France). A 100 mg kg^{-1} aqueous multielemental stock solution (Merck, Darmstadt, Germany) was used to prepare a standard solution at 10 mg kg^{-1} of Ca, Cr, Cu, Fe, K, Mg, Mn, Na, Pb and Zn. This later solution was used for optimization of the operating conditions studied and to evaluate the matrix effect caused by 15 acid solutions, which contained 2, 5 and 10% w/w of nitric acid (69% w/w), sulfuric acid (96% w/w), hydrochloric acid (37% w/w), and mixtures of these acids. The three different acids were supplied by Sigma-Aldrich (St. Louis, MO, USA). Six oil and fat samples were chosen to validate the methodology: *(i)* a used cooking oil, UCO, before and after a filtration step (density: 921 and 920 g L^{-1}, respectively); *(ii)* an animal fat, AF, before and after a filtration step (density: 920 and 916 g L^{-1}, respectively); and, *(iii)* a corn oil, CO, before and after a filtration step (density: 926 and 952 g L^{-1}, respectively).

The samples were mineralized following the UOP 389-15 method [24]. In this method the sample was treated with concentrated sulfuric acid to reduce the volatility of the metals, then coked at 500 °C for 12 h, and ashed at 538 °C. The residue was treated with aqua regia, and, after evaporation, it was dissolved in Milli-Q water. The analyte quantification was carried out by means of an external calibration methodology using 6 aqueous standards in a concentration range going from 0.1 to 50 mg kg^{-1}. Yttrium stock solution (1000 mg kg^{-1}, Merck, Darmstadt, Germany) was used as internal standard. A given volume of the Yttrium stock solution was added to the standards and samples to reach a final concentration of 10 mg kg^{-1}.

2.1.1. Instrumentation

Atomic and ionic intensities were measured by using an Agilent 4200 MP-AES instrument (Agilent Technologies, CA, USA) with an axial viewing. The sample introduction system consisted of a glass pneumatic concentric nebulizer (TR-30-A1, Meinhard® Glass Products, Santa Ana, USA) and a high temperature Torch Integrated Sample Introduction System (hTISIS) [23], equipped with a 47 cm^3 single-pass spray chamber. A conventional double-pass cyclonic spray chamber coupled to the same pneumatic concentric nebulizer was taken as a reference system. The operating conditions for both configurations are summarized in Table 1.

The nebulizer gas pressure and the viewing position were automatically optimized, for each analyte separately by means of the instrument software (MP Expert).

3. Results and discussion

In the present work, the sample was continuously delivered to the

Table 1
Operating conditions and line characteristics used for the analysis with the MIP-OES instrument for the hTISIS and a conventional sample introduction system.

Instrument parameter		Operating condition
Microwave Power (kW)		1.0
Plasma flow rate (L min^{-1})		20
Auxiliary flow rate (L min^{-1})		1.5
Read time (s)		3
Stabilization time (s)		15
Replicates		5
Element and type of line	**Emission wavelength (nm)**	**Excitation energy (eV)**
Ca II	422.673	2.93
Cr I	425.433	2.91
Cu I	324.754	3.82
Fe I	302.064	4.10
Fe I	358.119	4.32
Fe I	371.993	3.33
Fe I	382.588	4.15
Fe I	385.991	3.21
Fe I	404.581	4.55
K I	766.491	1.62
Mg I	285.213	4.85
Mn I	403.076	3.07
Na I	589.592	2.10
Pb I	405.781	4.38
Y II	371.029	3.52
Zn I	213.857	5.80

instrument. This made it possible to develop procedures for routine automated analysis. The critical variables studied were the nebulizer gas and liquid flow rates as well as the hTISIS chamber temperature. After preliminary tests, the impact of inorganic acids on the performance of the system was evaluated. Finally, the analysis of oils and fatty acid derivates after an acid digestion was selected as an example of the application field of hTISIS and MIP-OES. The studied elements (Table 1) were selected because they are of interest in the analysis of oil and fat samples. Moreover, the list of elements included easily and non-easily ionized elements.

3.1. Effect of the hTISIS critical variables on emission intensity

The impact of the nebulizer gas (nitrogen) flow rate, Q_g, on MIP-OES emission intensity is highlighted in Fig. 1. It may be observed that, for the hTISIS operated at 200 °C (473 K), the intensity increased with this variable up to 0.8 L min^{-1}. A plateau was reached above this value. This trend was a compromise between an increase in the aerosol transport efficiency (trend found at low Q_g values) and a shortening in the aerosol plasma residence time together with a decrease in the plasma excitation conditions (signal stabilization encountered at high values of the gas flow). The optimum values of the nebulizer gas flow rate corresponded to 0.8–1.0 L min^{-1} when the hTISIS was coupled to the instrument. The sequential character of the spectrometer allowed selecting a particular Q_g for each element. In fact, optimum value of this variable was 1.0 L min^{-1} for Ca, Cr, Fe, K, Mn, Na, Pb and Zn. Meanwhile, in the case of Cu and Mg, 0.9 L min^{-1} was the selected value whereas, for Y determination, this variable was set at 0.8 L min^{-1}.

An interesting point emerged when compared the optimum Q_g value found in MIP-OES with those encountered in ICP-OES and ICP-MS. When using the hTISIS, the respective values were 0.1–0.4 and 0.4–0.8 L min^{-1}, while 1 L min^{-1} was applied when the conventional sample introduction system was used [22,25]. This fact suggested that, with the MIP-OES instrument employed, the impact of a high temperature sample introduction system on its performance was less remarkable than when an argon plasma was under study. The reason of this behavior may lie in the higher thermal conductivity of nitrogen-based plasmas compared to argon-based ones, because for the former plasmas a higher number of collisions among electrons, ions and neutrals species may occur, thus reaching the local thermodynamic equilibrium state in a faster way [13].

The impact of the hTISIS temperature on the instrument performance

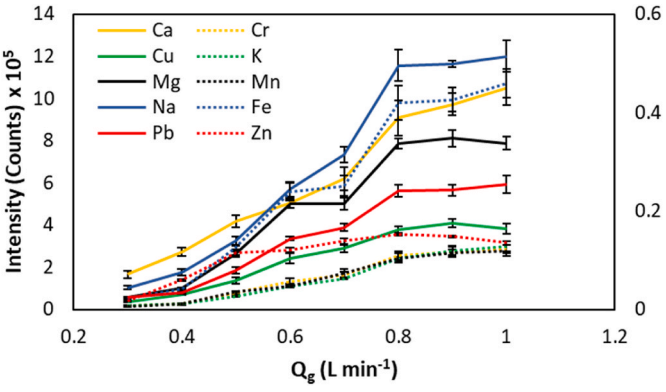

Fig. 1. Emission intensity (mean ± standard deviation) as a function of the nebulizer gas flow rate. hTISIS temperature: 200 °C, Liquid flow rate 60 μL min^{-1}. MIP-OES operating conditions described in Table 1. Primary axis: Ca, Cr, Cu, K, Mg and Mn; Secondary axis: Fe, Pb and Zn.

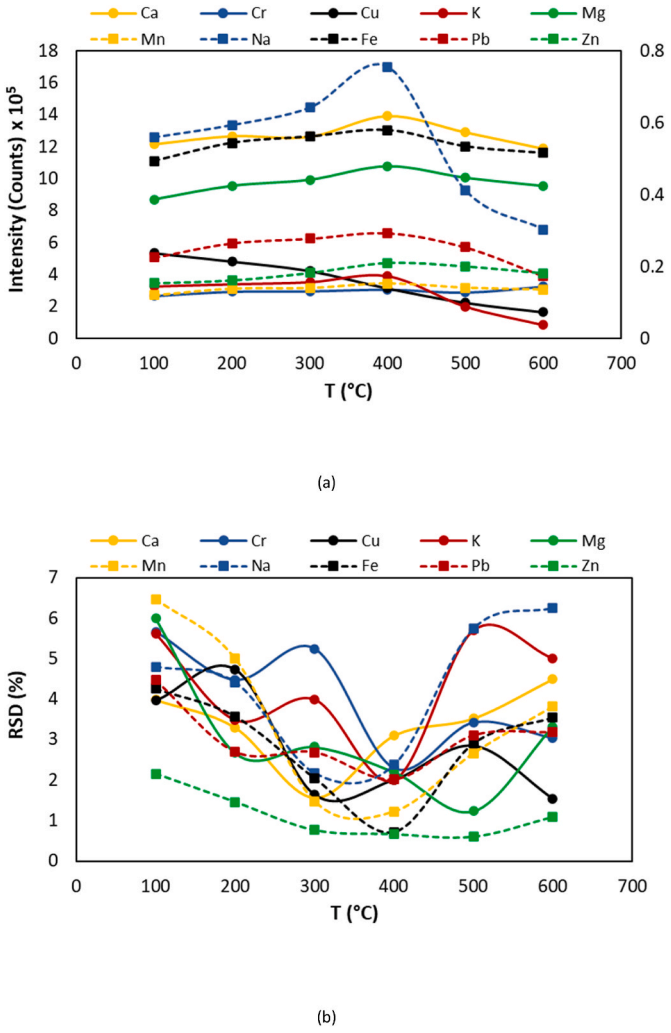

Fig. 2. Emission intensity (a) and RSD (b) as a function of the hTISIS temperature. Nebulizer gas flow rate: 0.9–1 L min^{-1}; liquid flow rate 60 μL min^{-1}. MIP-OES operating conditions described in Table 1. Primary axis: Ca, Cr, Cu, K, Mg and Mn; Secondary axis: Fe, Pb and Zn.

was subsequently studied. Fig. 2(a) shows the variation of the emission signal as a function of the hTISIS temperature for the mentioned gas flow rates. It was found that for most of them, the chamber temperature induced a moderate increase of signal at temperatures from 100 (373 K) to 400 °C (673 K). Above this value, the analytical magnitude went down. Moreover, it was observed that too a low or a high hTISIS temperature led to a degradation in the signal stability (Fig. 2(b)). Therefore, 400 °C (673 K) was the selected value, because this represented a good compromise between both the magnitude of the intensity and the relative standard deviation.

The third studied variable was the sample flow rate. The behavior of the signal versus Q_l depended strongly on the element considered (Fig. 3 (a)). Thus, for instance, signal for Mg peaked at 60 μL min^{-1}, whereas that for Mn and Cu showed a quite flat response. Interestingly, intensity for Ca had a maximum value at 150 μL min^{-1} and that for K increased with Q_l up to 200 μL min^{-1}. In the case of Na, the detector became saturated, and signals were not registered above 125 μL min^{-1}. As expected, the higher the liquid flow rate, the lower the signal RSD (Fig. 3 (b)) [26].

3.2. Comparison with a conventional sample introduction system

In order to discern whether this high temperature system resulted advantageous, a comparison was established with a conventional sample introduction device consisting in a pneumatic concentric nebulizer adapted to a double-pass cyclonic spray chamber.

In the case of the conventional sample introduction system, the chosen gas flow rate corresponded to that recommended by the manufacturer, which provided the highest sensitivity. This parameter was located, as in the case of the hTISIS, at values from 0.8 to 1.0 L min^{-1}. Likewise, the default liquid flow rate was 250 μL min^{-1}, 2.5 times higher than for the hTISIS. Fig. 4 shows the variation of the hTISIS (operated at variable Q_l values) to conventional system (at its optimum value). It was observed that at 20–40 μL min^{-1} the hTISIS provided similar sensitivities to those afforded by the conventional system but at a liquid flow rate from roughly 6 to 12 times higher. Only an improvement of the sensitivity was found for Fe, Pb and Zn. At 100 μL min^{-1}, the hTISIS supplied MIP-OES signals from 2 times (Mg and Cu) to around 19 times (Ca and K) higher than the conventional device. This was a clear advantage of the increased analyte transport efficiency induced by the work at high chamber temperatures. The limit of quantification was calculated according to equation (1):

$$LOQ = \frac{10\, s_b}{m} \quad (1)$$

where s_b corresponded to the standard deviation of ten consecutive blank measurements and m was the slope of the calibration line.

In agreement with the increase in sensitivity, the values of this parameter were significantly lower for the high temperature system than for the conventional one (Table 2). For elements such as Cr, K, Pb and Zn, the improvement factor was higher than one order of magnitude. This was in full agreement with the background equivalent concentration (BEC), because the hTISIS provided lower values than the cyclonic spray chamber. Moreover, the high temperature system was compared to the routine analysis UOP 389-15 method recommended by ASTM for the determination of trace metals in organic matrices such as oils and fatty acid derivatives [24] which employed an ICP-OES as a detection system. It is interesting to note that the combination of the hTISIS and MIP-OES allowed to achieve lower LOQ values than those encountered for the ICP-OES method.

Wash out times were also evaluated. Fig. 5 plots the signal recordings when introducing ultrapure water into the instrument after running a 10 mg kg^{-1} standard. Three different situations were considered: the conventional sample introduction setup at the recommended Q_l (250 μL min^{-1}) and the hTISIS at two different liquid flow rates (20 and 60 μL min^{-1}). At 250 μL min^{-1}, the time required to achieve a signal equal to 5% of the steady state intensity with the conventional device was longer than 30 s. This wash out time was similar to that required with the hTISIS but operated at 20 μL min^{-1}. When the latter device was set at 60

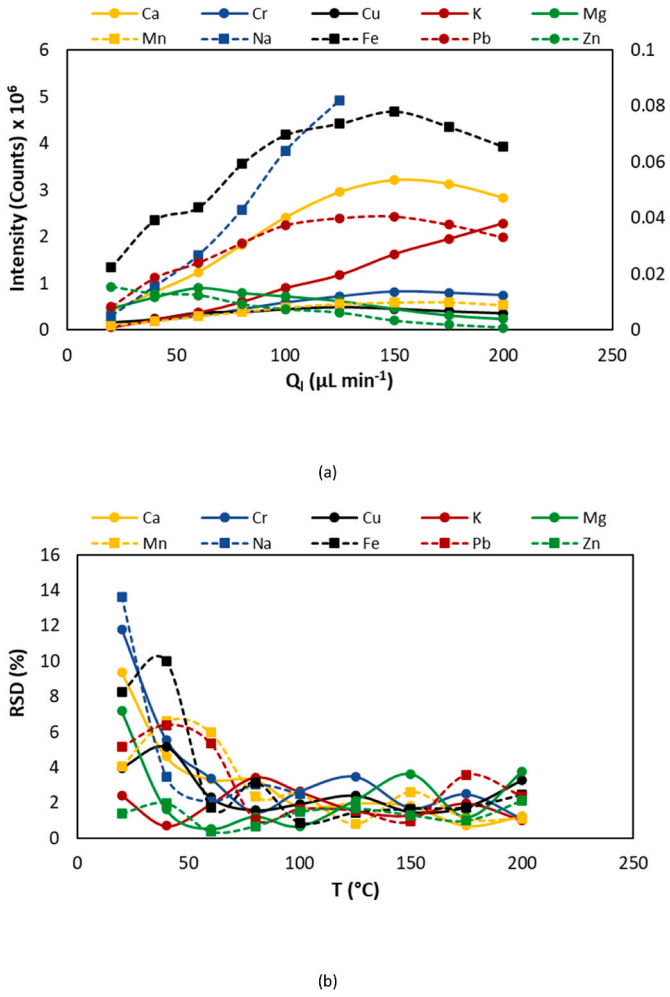

Fig. 3. Emission intensity (a) and signal RSD (b) as a function of the liquid flow rate. hTISIS temperature: 400 °C, Nebulizer gas flow rate: 0.9–1 L min^{-1}. MIP-OES operating conditions described in Table 1. Primary axis: Ca, Cr, Cu, K, Mg and Mn; Secondary axis: Fe, Pb and Zn.

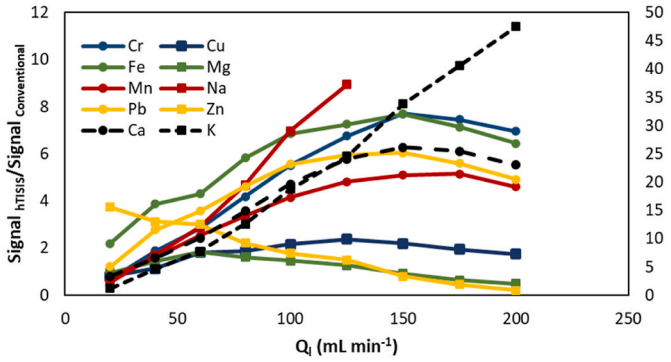

Fig. 4. Signal measured for the hTISIS relative to that for the conventional sample introduction system versus the liquid flow rate for representative elements. hTISIS: T = 400 °C; Q_g = 0.8–1.0 L min^{-1}. Conventional system: Q_l = 250 μL min^{-1}; Q_g = 0.9–1.0 L min^{-1}. MIP-OES operating conditions described in Table 1. Primary axis: Cr, Cu, Fe, Mg, Mn, Pb and Zn; Secondary axis: Ca and K.

Table 2
Relative sensitivity enhanced factor incorporated by the hTISIS with respect to the conventional sample introduction system, limits of quantification and background equivalent concentration provided by the devices evaluated. hTISIS: T = 400 °C; Q_l = 250 μL min^{-1}; Q_g = 0.8–1.0 L min^{-1}. Conventional system: Q_l = 250 μL min^{-1}; Q_g = 0.9–1.0 L min^{-1}. MIP-OES operating conditions described in Table 1.

Element	Sensitivity enhancement factor	LOQ (μg kg^{-1})			BEC (μg kg^{-1})	
	hTISIS/Conv	hTISIS	Conv	UOP 389-15[24]	hTISIS	Conv
Ca	26	21	70	80	13	450
Cr	32	1.2	18	40	21	360
Cu	2.4	4	3	10	260	190
Fe	7.7	15	78	90	220	3000
K	47	11	130	50	29	890
Mg	1.8	3	3	40	93	62
Mn	5.2	0.9	3	10	20	110
Na	8.9	5	27	40	26	110
Pb	6.0	30	130	40	350	3400
Zn	3.7	360	1300	30	28,000	17,000

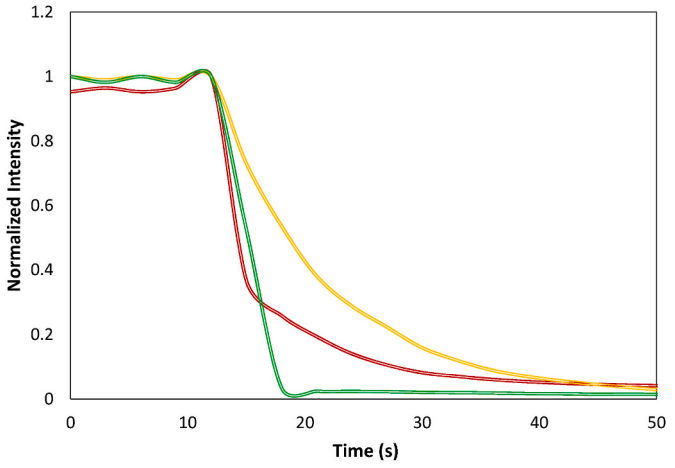

Fig. 5. Calcium signal variation versus time when switching from a 10 mg kg^{-1} to ultrapure water. Red: Conventional sample introduction system, Q_l (conventional system): 250 μL min^{-1}; Green: hTISIS, Q_l: 60 μL min^{-1}; and, Yellow: hTISIS, Q_l: 20 μL min^{-1} hTISIS: T = 400 °C; Q_g = 0.8–1.0 L min^{-1}. Conventional system: Q_g = 0.9–1.0 L min^{-1}. MIP-OES operating conditions described in Table 1. (For interpretation of the references to colour in this figure legend, the reader is referred to the Web version of this article.)

μL min^{-1}, the wash out time was shorter than 10 s. This clearly highlighted another interesting advantage of the hTISIS, which implied that the chamber walls remained dry, thus minimizing solution re-nebulization.

3.3. Matrix effects caused by inorganic acids

Inorganic acids such as nitric, hydrochloric and sulfuric may cause strong MIP-OES interferences thus leading to inaccurate results. In order to determine the extent of the interference, the so-called relative intensity, I_{rel}, has been calculated according to:

$$I_{rel} = \frac{Emission\ intensity^{Matrix\ j}_{Element\ i}}{Emission\ intensity^{Water}_{Element\ i}} \quad (2)$$

The I_{rel} target value was 1, *i.e.*, sensitivities were the same for a given matrix and a sample containing only water as solvent. Two different sets of matrices were evaluated: those containing increasing concentrations of single acids (*i.e.*, nitric, sulfuric and hydrochloric) and binary mixtures of nitric acid with either sulfuric or hydrochloric acid.

3.3.1. Single acid matrices

There are relatively few systematic studies about the impact of inorganic acids on the MIP-OES performance [7]. Inorganic acids in fact have proven to cause non spectral interferences in MIP-OES [27]. These species are commonly present as a result of a previous digestion step of an organic sample such as petroleum products [28].

Fig. 6 shows the I_{rel} values found for solutions containing either nitric (a), sulfuric (b) or hydrochloric (c) acid. When considering the conventional sample introduction system (full bars), it was observed that the I_{rel} values depended on the acid present and the element measured. However, it could be stated that this parameter took values below 1 for virtually all the situations evaluated. The higher the acid concentration, the lower the I_{rel}, and that the effect appeared to be slightly more severe for sulfuric than for nitric or hydrochloric, likely due to the higher values of some physical chemical properties (density and viscosity) of the former acid which can induce the generation of coarse aerosols. Interestingly, it was encountered that the extent of the matrix effect was similar to that encountered in ICP-OES [29,30].

Globally speaking, the results for the conventional sample introduction system illustrated a negative interference that could be due to two main reasons: *(i)* changes in the plasma thermal characteristics; and, *(ii)* modifications in the performance of the sample introduction system. In order to try to evaluate the first point, the plasma excitation temperature was determined in presence and in absence of the evaluated matrices. Plasma excitation temperature could be defined as the temperature prevailing the population density of atomic level p which follows a Boltzmann distribution [31]. To obtain this parameter, six different iron emission lines were selected (see Table 1). Using the Boltzmann law (3) a straight line was obtained whose slope was inversely proportional to the plasma excitation temperature.

$$\mathrm{In}\left(\frac{I_{pq}}{g_p A_{pq}}\right) = \frac{-E_{pq}\lambda_{pq}}{kT_{exc}} + In\left(\frac{ndhc}{4\pi Z}\right) \quad (3)$$

Fig. 7 illustrates that the matrix nature did modify the value of T_{exc} neither when using the conventional sample introduction system nor when the hTISIS was under study. These results demonstrated that the effect of inorganic acids on the MIP-OES sensitivity was induced by a change in the aerosol transport efficiency. When comparing the T_{exc} supplied by both devices, it clearly emerged that the hTISIS led to a decrease in this plasma fundamental parameter as compared to the conventional setup. The higher amount of solution delivered to the excitation cell was, thus, in the origin of this result.

Following the comparison between sample introduction systems, Fig. 6 indicated that I_{rel} was closer to 1 when using the hTISIS than for the conventional design. This result was expected, considering that acids induced a change in aerosol transport parameters. The aerosol transport efficiency with the hTISIS reaches values close to 100% regardless the matrix nature [23,32]. In absence of plasma changes, the emission intensity was, hence, the same for acids and water, thus, as it has been observed in both ICP-OES [25,33] and ICP-MS [34], the use of the hTISIS was beneficial from the point of view of matrix effect removal, also for MIP-OES.

3.3.2. Binary mixtures containing nitric acid

MIP-OES has been used for the analysis of complex matrices requiring from a previous digestion based on the use of a mixture of inorganic acids such as nitric and hydrochloric. Therefore, the possibility of introducing combined acid matrices was evaluated. The obtained results are included in Fig. 8 for mixtures containing nitric and sulfuric (a) or hydrochloric (b) acid. Similar results as for single-acid matrices were obtained. I_{rel} values were closer to 1 when the hTISIS was operated than for the conventional device. Only a few exceptions

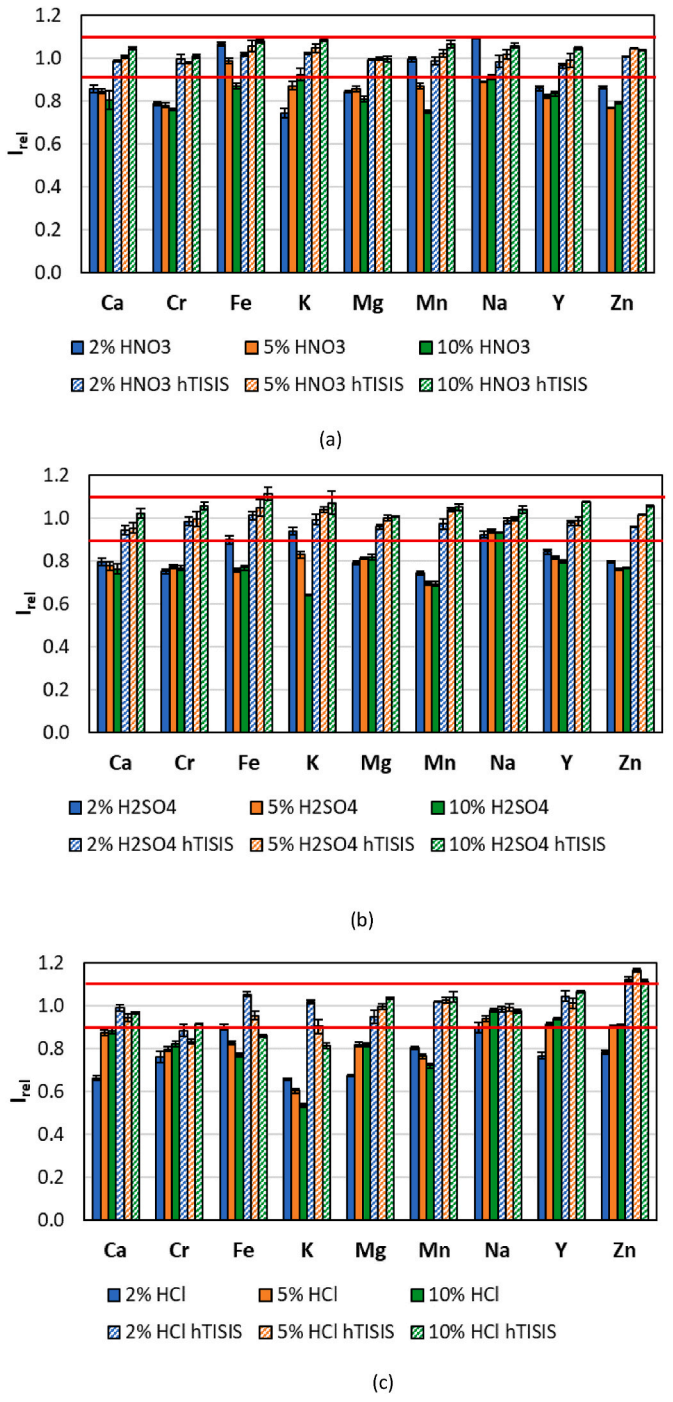

Fig. 6. Relative intensities (I_{rel}; mean ± standard deviation) for single acid solutions containing (a) nitric acid; (b) sulfuric acid; and, (c) hydrochloric acid. hTISIS operating conditions: T = 400 °C; Q_l = 100 μL min^{-1}; Q_g = 0.8 (Y); 0.9 (Cu and Mg); 1.0 (Ca, Cr, Fe, K, Mn, Na and Zn) L min^{-1}. Conventional system operating conditions: Q_l = 250 μL min^{-1}; Q_g = 0.65 (K, Mn and Na), 0.75 (Fe, Y and Zn); 0.9 (Ca, Cr and Mg) L min^{-1}. MIP-OES operating conditions described in Table 1. Red lines indicated 0.9 and 1.1 recovery values. (For interpretation of the references to colour in this figure legend, the reader is referred to the Web version of this article.)

were found. For instance, relative intensity values found for K, Fe and Mn in a mixture containing 10% nitric and sulfuric acid were 1.16 ± 0.02; 1.15 ± 0.01, and 1.15 ± 0.02, respectively. When matrix was a mixture of nitric and hydrochloric acid, the exceptions found were Cr (5% HNO_3 + HCl), Y (10% HNO_3 + HCl) and Zn (2% HNO_3 + HCl),

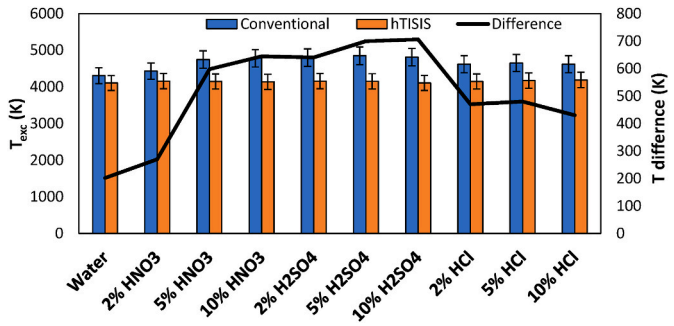

Fig. 7. Excitation temperature (mean ± standard deviation) for the different matrices and the two evaluated sample introduction systems. hTISIS operating conditions: T = 400 °C; Q_l = 100 μL min^{-1}; Q_g = 1.0 L min^{-1}. Conventional system operating conditions: Q_l = 250 μL min^{-1}; Q_g = 0.75 L min^{-1}. MIP-OES operating conditions described in Table 1.

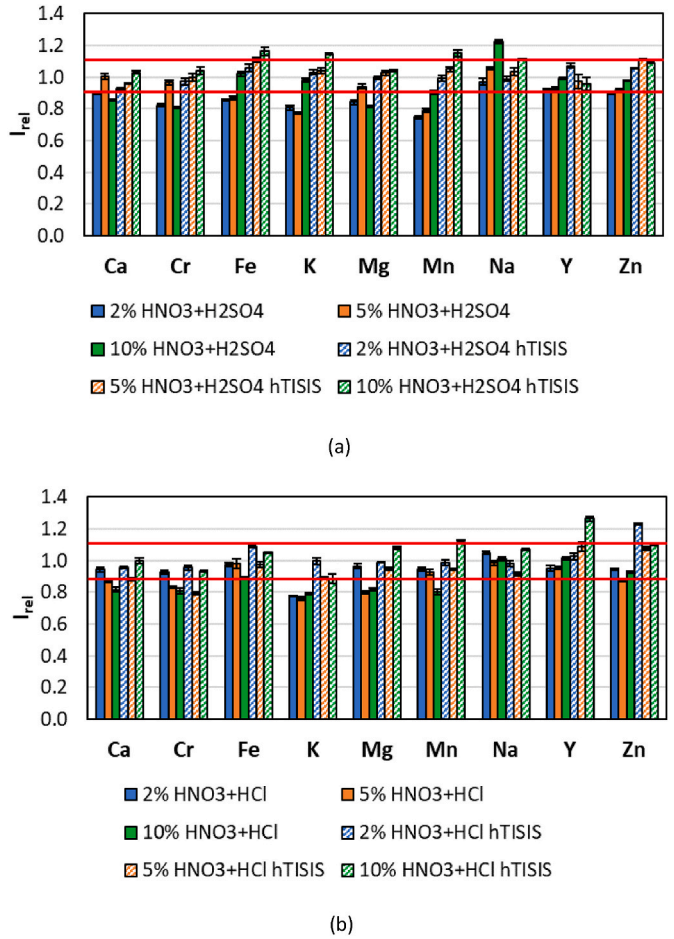

Fig. 8. Relative intensities (I_{rel}; mean ± standard deviation) for binary solutions containing nitric acid and (a) sulfuric acid; and, (b) hydrochloric acid. hTISIS (dashed bars) operating conditions: T = 400 °C; Q_l = 100 μL min^{-1}; Q_g = 0.8 (Y); 0.9 (Cu and Mg); 1.0 (Ca, Cr, Fe, K, Mn, Na and Zn) L min^{-1}. Conventional system (full bars) operating conditions: Q_l = 250 μL min^{-1}; Q_g = 0.65 (K, Mn and Na), 0.75 (Fe, Y and Zn); 0.9 (Ca, Cr and Mg) L min^{-1}. MIP-OES operating conditions described in Table 1. Red lines indicated 0.9 and 1.1 recovery values. (For interpretation of the references to colour in this figure legend, the reader is referred to the Web version of this article.)

where the relative intensities values were 0.80 ± 0.01; 1.26 ± 0.01, and 1.23 ± 0.02, respectively.

3.4. Analysis of real samples

Based on the above discussed results, six different samples were analyzed, as an example of one of the application fields. Samples corresponded to biofuel feedstock before and after their filtration in the refining process. In order to perform these experiments, once mineralized, the resulting solutions were introduced into the MIP-OES apparatus using the hTISIS sample introduction system. Then external calibration from aqueous standards was performed. To simulate the matrix of the mineralized samples, the standards and the blank solutions were prepared in a 3% (w/w) HCl solution. The standard deviation of this blank solution was used to calculate the procedural LOQs. For this reason, LOQs showed in Table 3 were different than those reported in Table 2, which were obtained using a Milli-Q water as a blank.

The samples were also analyzed in accordance with the UOP 389-15 method [24]. After mineralization, samples were analyzed by ICP-OES, employing a conventional sample introduction system. This methodology was taken as the reference one to compare the concentration results obtained by MIP-OES. Table 3 shows the concentration results obtained by both analytical methodologies for a set of 6 samples: a used cooking oil (UCO), an animal fat (AF), and a corn oil (CO), the three of them before and after suffering a filtration step. Only those elements quantified in the samples have been included in Table 3. It should be noted that the reference methodology presented higher variances than those encountered for hTISIS and MIP-OES methodology. Concentrations obtained according to both analytical methodologies were statistically compared. F-test was applied to evaluate statistical differences in terms of variance between both methodologies. When variances could be considered statistically comparable, the concentration obtained were evaluated by means of the t-Student test. If the variances were not statistically comparable, t-value and the degree of freedom were calculated by applying the following equations:

$$t = \frac{(\bar{x}_1 - \bar{x}_2)}{\sqrt{\frac{s_1^2}{n_1} + \frac{s_2^2}{n_2}}} \quad (4)$$

$$Degrees\ of\ freedom = \frac{\left(\frac{s_1^2}{n_1} + \frac{s_2^2}{n_2}\right)^2}{\left(\frac{s_1^4}{n_1^2(n_1-1)} + \frac{s_2^4}{n_2^2(n_2-1)}\right)} \quad (5)$$

Where $\bar{x}$ was the mean value, s was the standard deviation and n was the number of replicates of method 1 or 2. As it can be observed in Table 3, Table S1 and Table S2 with a few exceptions, the concentrations obtained according to both analytical methodologies were statistically similar. Statistically different results were provided by both methods only in 8 out of the 48 evaluated cases.

In general terms, it can be observed that the use of a filtration step can reduce the amount of analytes present in the raw samples in high concentrations (*e.g.*, Ca, Fe and Mg in the animal fat sample), however the process reduces its efficiency when the concentration of the element is low (several mg kg^{-1}), implying sometimes the increase of the analyte concentration as it is reported in the UCO sample for Fe.

Focusing on the analyte content for each sample, alkali and alkaline earth metals are present in the 6 samples at high proportions (>10 mg kg^{-1}), since these elements are present in the raw materials, such as seeds used for the oil production [35]. Furthermore, Fe was detected at high concentration in the animal fat sample likely due to the transfer from some components made of stainless steel used to collect the fat [21].

The control of these elements (Ca, Fe, K, Mg and Na) is important for the biofuel production because they can carry out corrosion issues. Alkaline earth elements can generate insoluble soap, clogging and

Table 3
Elemental concentrations (mg kg^{-1}) found for the used cooking oil samples (UCO), the animal fat samples (AF), and the corn oil samples (CO), before and after filtration (af). (n.a.: not available). Concentration has been expressed as mean ± standard deviation.

	UCO hTISIS MIP-OES	UCO Mineralization ICP-OES	UCO-af hTISIS MIP-OES	UCO-af Mineralization ICP-OES	AF hTISIS MIP-OES	AF Mineralization ICP-OES	AF-af hTISIS MIP-OES	AF-af Mineralization ICP-OES	CO hTISIS MIP-OES	CO Mineralization ICP-OES	CO-af hTISIS MIP-OES	CO-af Mineralization ICP-OES
Ca	**1.96 ± 0.07**	**2.1 ± 0.6**	**1.15 ± 0.06**	**1.15 ± 0.07**	**Saturated**	**950 ± 20**	9.98 ± 0.12	5.6 ± 0.2	2.84 ± 0.18	1.3 ± 0.3	2.7 ± 0.3	1.35 ± 0.07
Fe	**1.11 ± 0.04**	**1.3 ± 0.4**	3.19 ± 0.09	2.10 ± 0.07	**18.1 ± 0.5**	**21.2 ± 1.3**	**0.54 ± 0.02**	**0.54 ± 0.01**	0.74 ± 0.02	0.35 ± 0.07	0.67 ± 0.03	0.38 ± 0.02
K	**18 ± 2**	**13 ± 7**	**10.9 ± 0.5**	**12 ± 7**	**Saturated**	**160 ± 40**	**52 ± 4**	**50 ± 30**	17.2 ± 0.8	n.a.	17.8 ± 1.5	12 ± 2
Mg	**0.94 ± 0.07**	**0.8 ± 0.2**	**0.44 ± 0.03**	**0.42 ± 0.02**	19.5 ± 1.6	48 ± 9	**0.84 ± 0.03**	**0.60 ± 0.02**	**11.6 ± 1.0**	**13 ± 3**	**11.7 ± 0.4**	**12.8 ± 0.6**
Mn	**< 0.013**	**0.020 ± 0.007**	**0.44 ± 0.06**	**0.45 ± 0.04**	**0.47 ± 0.03**	**0.34 ± 0.09**	**< 0.013**	**0.010 ± 0.004**	**< 0.013**	**0.04 ± 0.01**	**< 0.013**	**0.050 ± 0.010**
Na	**Saturated**	**20 ± 13**	**10.4 ± 0.5**	**11.3 ± 10.7**	**Saturated**	**230 ± 80**	**Saturated**	**61 ± 4**	Saturated	n.a.	Saturated	n.a.

deposit formation within the engine and fuel system. Moreover, Ca, Fe and Mg may increase the oxidative decomposition of oils, fats, and the biofuels themselves, generating residues leading to fuel filters blocking, and Mn is also responsible for corrosion. However, these elements were present at concentrations below 1 mg kg^{-1} in all the sample analyzed [1].

4. Conclusions

In this work, the use of the high temperature sample introduction system (hTISIS) adapted to MIP-OES is reported for the first time and provides excellent analytical performance for the analysis of aqueous samples according to a continuous sample aspiration regime. This makes it possible to use this sample introduction device for routine analysis of liquid samples through MIP-OES. Therefore, hTISIS may expand the field of application to microwave plasmas for the elemental analysis of liquid samples.

After an optimization of the different operating conditions, the hTISIS at 400 °C coupled to MIP-OES showed several advantages over the conventional setup: (*i*) better LOQs; (*ii*) lower wash out times; and (*iii*) mitigation of matrix effects in a series of acid digested samples. LOQs obtained with this previous configuration were one order of magnitude lower than those for a conventional sample introduction system. Moreover, LOQs were lower or similar to those encountered in common ICP-OES applications.

As it has been previously reported for ICP-OES and ICP-MS, the hTISIS was able to overcome matrix effects caused by inorganic acids. With this sample introduction system, negligible matrix effects were observed in the analysis of acid digested samples by MIP-OES. Thus, it was possible to perform accurate analysis by applying external calibration using a set of standards prepared in 3% (w/w) HCl solution.

CRediT authorship contribution statement

Santiago Martínez: Methodology, Formal analysis, Writing – original draft. **Raquel Sánchez:** Conceptualization, Methodology, Formal analysis, Writing – original draft, Writing – review & editing, Supervision. **José-Luis Todolí:** Conceptualization, Formal analysis, Writing – original draft, Writing – review & editing, Supervision, Project administration.

Declaration of competing interest

The authors declare that they have no known competing financial interests or personal relationships that could have appeared to influence the work reported in this paper.

Data availability

Data will be made available on request.

Appendix A. Supplementary data

Supplementary data to this article can be found online at https://doi.org/10.1016/j.aca.2023.340948.

References

[1] S. Martínez, R. Sánchez, J. Lefevre, J.L. Todolí, Multi-elemental analysis of oil renewable fuel feedstock, Spectrochim. Acta - Part B at, Spectroscopy (Ott.) 189 (2022), 106356, https://doi.org/10.1016/j.sab.2021.106356.

[2] R.S. Amais, G.L. Donati, D. Schiavo, J.A. Nóbrega, A simple dilute-and-shoot procedure for Si determination in diesel and biodiesel by microwave-induced plasma optical emission spectrometry, Microchem. J. 106 (2013) 318–322, https://doi.org/10.1016/j.microc.2012.09.001.

[3] R.C. Machado, A.B.S. Silva, G.L. Donati, A.R.A. Nogueira, Multi-energy calibration as a strategy for elemental analysis of fertilizers by microwave-induced plasma optical emission spectrometry, J. Anal. At. Spectrom. 33 (2018) 1168–1172, https://doi.org/10.1039/C8JA00077H.

[4] A.G. Althoff, C.B. Williams, T. McSweeney, D.A. Gonçalves, G.L. Donati, Microwave-induced plasma optical emission spectrometry (MIP OES) and standard dilution analysis to determine trace elements in pharmaceutical samples, Appl. Spectrosc. 71 (2017) 2692–2698, https://doi.org/10.1177/0003702817721750.

[5] V. Balaram, V. Dharmendra, P. Roy, C. Taylor, C.T. Kamala, M. Satyanarayanan, P. Kar, K.S.V. Subramanyam, A.K. Raju, A. Krishnaiah, Analysis of geochemical samples by microwave plasma-AES, At. Spectrosc. 35 (2014) 65–78, https://doi.org/10.46770/AS.2014.02.003.

[6] C. Vella, E. Attard, Consumption of minerals, toxic metals and hydroxymethylfurfural: analysis of infant foods and formulae, Toxics 7 (2019) 4–11, https://doi.org/10.3390/toxics7020033.

[7] V. Balaram, Microwave plasma atomic emission spectrometry (MP-AES) and its applications – a critical review, Microchem. J. 159 (2020), 105483, https://doi.org/10.1016/j.microc.2020.105483.

[8] R. Serrano, E. Anticó, G. Grindlay, L. Gras, C. Fontàs, Determination of elemental bioavailability in soils and sediments by microwave induced plasma optical emission spectrometry (MIP-OES): matrix effects and calibration strategies, Talanta 240 (2022), 123166, https://doi.org/10.1016/j.talanta.2021.123166.

[9] Z. Zhang, K. Wagatsuma, Comparison of the analytical performance of high-powered, microwave-induced air plasma and nitrogen plasma atomic emission spectrometry, J. Anal. At. Spectrom. 17 (2002) 699–703, https://doi.org/10.1039/B202777C.

[10] J. Nelson, G. Gilleland, L. Poirier, D. Leong, P. Hajdu, F. Lopez-Linares, Elemental analysis of crude oils using microwave plasma atomic emission spectroscopy, Energy Fuel. 29 (2015) 5587–5594, https://doi.org/10.1021/acs.energyfuels.5b01026.

[11] A. Müller, D. Pozebon, A. Schwingel Ribeiro, Methodology for elemental analysis of a mineral fertilizer, some of its raw materials and limestone using microwave-induced plasma optical emission spectrometry (MIP OES), Anal. Methods 12 (2020) 2638–2644, https://doi.org/10.1039/D0AY00459F.

[12] N. Chalyavi, P.S. Doidge, R.J.S. Morrison, G.B. Partridge, Fundamental studies of an atmospheric-pressure microwave plasma sustained in nitrogen for atomic emission spectrometry, J. Anal. At. Spectrom. 32 (2017) 1988–2002, https://doi.org/10.1039/C7JA00159B.

[13] D.A. Goncalves, T. McSweeney, G.L. Donati, Characteristics of a resonant iris microwave-induced nitrogen plasma, J. Anal. At. Spectrom. 31 (2016) 1097–1104, https://doi.org/10.1039/C6JA00066E.

[14] K. Jankowski, E. Reszke, Recent developments in instrumentation of microwave plasma sources for optical emission and mass spectrometry: tutorial review, J. Anal. At. Spectrom. 28 (2013) 1196–1212, https://doi.org/10.1039/C3JA50110H.

[15] K.M. Thaler, A.J. Schwartz, C. Haisch, R. Niessner, G.M. Hieftje, Preliminary survey of matrix effects in the microwave-sustained, inductively coupled atmospheric-pressure plasma (MICAP), Talanta 180 (2018) 25–31, https://doi.org/10.1016/j.talanta.2017.12.021.

[16] R. Serrano, G. Grindlay, L. Gras, J. Mora, Evaluation of calcium-, carbon- and sulfur-based non-spectral interferences in high-power MIP-OES: comparison with ICP-OES, J. Anal. At. Spectrom. 34 (2019) 1611–1617, https://doi.org/10.1039/C9JA00148D.

[17] C.B. Williams, R.S. Amais, B.M. Fontoura, B.T. Jones, J.A. Nóbrega, G.L. Donati, Recent developments in microwave-induced plasma optical emission spectrometry and applications of a commercial Hammer-cavity instrument, TrAC - Trends Anal. Chem. 116 (2019) 151–157, https://doi.org/10.1016/j.trac.2019.05.007.

[18] S. Karlsson, V. Sjöberg, A. Ogar, Comparison of MP AES and ICP-MS for analysis of principal and selected trace elements in nitric acid digests of sunflower (Helianthus annuus), Talanta 135 (2015) 124–132, https://doi.org/10.1016/j.talanta.2014.12.015.

[19] E. Varbanova, V. Stefanova, A comparative study of inductively coupled plasma optical emission spectrometry and microwave plasma atomic emission spectrometry for the direct determination of lanthanides in water and environmental samples, Ecol. Saf. 9 (2015) 362–374.

[20] O.V. Pelipasov, E.V. Polyakova, Matrix effects in atmospheric pressure nitrogen microwave induced plasma optical emission spectrometry, J. Anal. At. Spectrom. 35 (2020) 1389–1394, https://doi.org/10.1039/D0JA00065E.

[21] S. Martínez, R. Sánchez, J. Lefevre, J.-L. Todolí, Multielemental analysis of vegetable oils and fats by means of ICP-OES following a dilution and shot methodology, J. Anal. At. Spectrom. 35 (2020) 1897–1909, https://doi.org/10.1039/D0JA00112K.

[22] A. Bazzano, K. Latruwe, M. Grotti, F. Vanhaecke, Lead isotopic analysis of Antarctic snow using multi-collector ICP-mass spectrometry, J. Anal. At. Spectrom. 30 (2015) 1322–1328, https://doi.org/10.1039/C4JA00484A.

[23] S. Martínez, R. Sánchez, J.L. Todolí, Inductively coupled plasma tandem mass spectrometry (ICP-MS/MS) for the analysis of fuels, biofuels and their feedstock using a high temperature total consumption sample introduction system operated under continuous sample aspiration mode, J. Anal. At. Spectrom. 37 (2022) 1032–1043, https://doi.org/10.1039/D2JA00024E.

[24] Honeywell UOP, UOP 389-15: Trace Metals in Organics by ICP-OES, 2015.

[25] C. Sánchez, C.P. Lienemann, J.L. Todolí, Metal and metalloid determination in bioethanol through inductively coupled plasma-optical emission spectroscopy, Spectrochim. Acta, Part B 115 (2016) 16–22, https://doi.org/10.1016/j.sab.2015.10.011.

[26] E. Paredes, M. Grotti, J.M. Mermet, J.L. Todolí, Heated-spray chamber-based low sample consumption system for inductively coupled plasma spectrometry, J. Anal. At. Spectrom. 24 (2009) 903–910, https://doi.org/10.1039/B904002A.

[27] E.V. Polyakova, Y.N. Nomerotskaya, A.I. Saprykin, Effect of matrix element and acid on analytical signals in nitrogen microwave-plasma atomic emission spectrometry, J. Anal. Chem. 75 (2020) 474–478, https://doi.org/10.1134/S1061934820040115.
[28] L. Poirier, J. Nelson, G. Gilleland, S. Wall, L. Berhane, F.A.L. Linares, Comparison of preparation methods for the determination of metals in petroleum fractions (1000°F +) by microwave plasma-atomic emission spectroscopy, Energy Fuels 31 (2017) 7809–7815, https://doi.org/10.1021/acs.energyfuels.7b00654.
[29] J.L. Todolí, J.M. Mermet, Effect of the spray chamber design on steady and transient acid interferences in inductively coupled plasma atomic emission spectrometry, J. Anal. At. Spectrom. 15 (2000) 863–867, https://doi.org/10.1039/B000589O.
[30] S. Maestre, J. Mora, J.L. Todolí, A. Canals, Evaluation of several commercially available spray chambers for use in inductively coupled plasma atomic emission spectrometry, J. Anal. At. Spectrom. 14 (1999) 61–67, https://doi.org/10.1039/A806550K.
[31] T. Hasegawa, H. Haraguchi, Fundamental properties of inductively coupled plasmas, in: A. Montaser, D.W. Golightly (Eds.), Inductively Coupled Plasmas in Analytical Atomic Spectrometry, VCH Publishers, New York, 1987, pp. 267–322.
[32] R. Sánchez, A. Cañabate, C. Bresson, F. Chartier, H. Isnard, S. Maestre, A. Nonell, J. L. Todolí, Comparison of a high temperature torch integrated sample introduction system with a desolvation system for the analysis of microsamples through inductively coupled plasma mass spectrometry, Spectrochim. Acta, Part B 129 (2017) 28–36, https://doi.org/10.1016/j.sab.2017.01.004.
[33] F. Ardini, M. Grotti, R. Sánchez, J.L. Todolí, Improving the analytical performances of ICP-AES by using a high-temperature single-pass spray chamber and segmented-injections micro-sample introduction for the analysis of environmental samples, J. Anal. At. Spectrom. 27 (2012) 1400–1404, https://doi.org/10.1039/C2JA30152K.
[34] C. Sánchez, C.P. Lienemann, J.L. Todolí, Analysis of bioethanol samples through Inductively Coupled Plasma Mass Spectrometry with a total sample consumption system, Spectrochim. Acta, Part B 124 (2016) 99–108, https://doi.org/10.1016/j.sab.2016.08.018.
[35] R. Sánchez, C. Sánchez, C.P. Lienemann, J.L. Todolí, Metal and metalloid determination in biodiesel and bioethanol, J. Anal. At. Spectrom. 30 (2015) 64–101, https://doi.org/10.1039/C4JA00202D.